MATEC Web of Conferences **86**, 01021 (2016) DOI: 10.1051/matecconf/20168601021
IPICSE-2016

Buckling resistance assessment of thin-walled open section element under pure compression

Andrzej Piotrowski[1], *Łukasz* Kowalewski[1*], *Radosław* Szczerba[1], *Marcin* Gajewski[1] and *Stanisław* Jemioło[1]

[1]WUT, Faculty of Civil Engineering, Armii Ludowej 16, 00-637 Warsaw, Poland

Abstract. The paper deals with the problem of buckling resistance determination in case of perforated thin-walled elements. Depending on element slenderness the limit load in compression mode may be determined taking into account elastic (LBA analysis), elasto-plastic and plastic material properties (GMNA analysis). The limit load value is determined on the basis of thin-walled open section beam theory in case of elastic buckling and using Johnson-Ostenfeld approximation for elasto-plastic buckling. Obtained results are compared with finite element solutions derived using shell modelling and large deformation theory with Huber-Mises elasto-plasticity constitutive model without any geometrical imperfections. Some results of the carried out experiments are also shown.

1 Introduction

In the paper the buckling resistance of the perforated thin-walled bar (without any geometrical imperfections) is under investigation. Analysed elements with the sigmoidal cross-section are used as a vertical support element for storage systems. Perforations are used as a supports for shelfs mounting elements and also as a mounting places for structure stiffening metal tie cables.

Depending on the distance between shelfs the slenderness for the analysed element is changing, leading to the elastic buckling or elasto-plastic load capacity problems. The limit load analysis was conducted with the use of thin-walled beam theory and compared with the results from the FEM analysis (shell models). In the case of analytical modelling with thin-walled beam theory the Johnson-Ostenfeld approximation has been used for the elastic-plastic range. In large deformation finite element shell models the material description is done in the frame of elasto-plasticity with flow rule associated with Huber-Mises yield condition and isotropic hardening. The main purpose of the paper is to compare the analytical solution for the perforated bar, for which perforations are taken into account through the concept of thinening of the bar wall (assuming equivalence of the material volume), with numerical solutions. Both analysis are done for perfect members, and finaly presented against some experimental tests done on imperfect samples with limited length (limitations of the testing systems). In the case of tested samples the geometrical and boundary type imperfections were identified.

* Corresponding author: l.kowalewski@il.pw.edu.pl

2 Material and geometry

The storage system elements are made from steel, which is treated as homogenous and isotropic material. The material parameters were determined based on uniaxial tensile tests carried out on three specimens cut out of the analysed structure in accordance with the standard [1]. The samples of 12mm width and 2mm thickness were tested using the Instron material testing system. The parameters determined on the basis of these tests are shown in Table 1. Such parameters are needed for analytical modelling (Johnson-Ostenfeld approximation). In case of parameters for Huber-Mises elasto plasticity additionaly the Poisson coefficient is assumed as equal to 0.3 and uniaxial tension test results are reproduced using elasto-plasticity model with isotropic isotropic strain hardening in wide range of strains. The dimensions of analysed element and its cross-section are shown in Figure 1.

Table 1. Material parameters.

Young's modulus E [GPa]	**Proportionality limit R_H [MPa]**	**Plasticity limit R_e [MPa]**
230.0	382.2	453.5

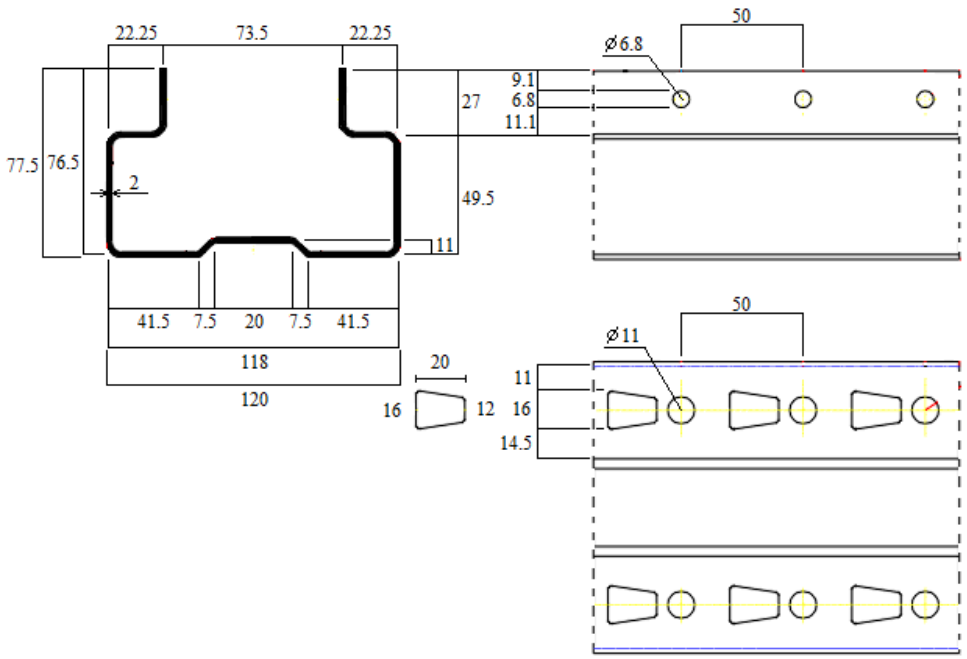

Fig. 1. Dimensions of analysed perforated element.

3 Determination of the compressive load capacity by the thin-walled beam theory

The perforated element shown in Figure 1 was replaced – according to [2] (chapter 8.3) – with the bar with equivalent cross-section, where the walls have been locally thinned in a way so as to keep the material volume (Figure 2).

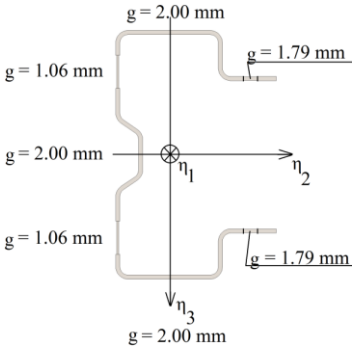

Fig. 2. Cross-section with thinned walls and rounded corners (g stands for wall thickness).

The computations were carried out for four types of element's cross-section: full cross-section (with filled perforations) and either rounded corners or simplified not-rounded corners (the latter one refered to as 'max' later on) or thinned cross-section (with perforations), again with either rounded ('min' later on) or not-rounded corners. In case of rounded corners – according to [3] – the geometrical cross-section characteristics are derived as:

$$A \approx A_k\left(1-\delta\right), \quad I \approx I_k\left(1-2\delta\right), \quad I_\omega \approx I_{\omega;k}\left(1-4\delta\right), \tag{1}$$

Where „k" index stands for characteristics of a cross-section with not-rounded corners. The δ parameter can be determined from:

$$\delta = 0.43\left(\sum_j R_j \frac{\varphi_j}{90^\circ}\right) / \left(\sum_i b_i\right), \tag{2}$$

Where: R – internal radius of rounding, φ – angle between the coincident walls (in degrees), b – the distance between the roundings' middle points.

The calculated geometrical characteristics are presented in Table 2, where No.1 stands for full and not-rounded, No.2 for full and rounded, No.3 for thinned and not-rounded and No.4 for thinned and rounded cross-section.

Table 2. Geometrical characteristics.

No.	**η_{2c}** [mm]	**η_{2A}** [mm]	**A** [mm^2]	**I_2** [mm^4]	**I_3** [mm^4]	**I_ω** [mm^6]	**I_s** [mm^4]
1	25.7	-57.1	654	1 321 104	388 392	1 952 013 679	872
2	25.2	-55.9	625	1 203 350	353 773	1 604 034 794	795
3	26.8	-59.4	621	1 268 536	363 541	1 848 685 312	789
4	26.2	-58.1	594	1 155 467	331 137	1 519 126 426	719

To determine the Kirchhoff modulus G = 88.46 MPa, the torsional stiffness $K_s = GI_s$ and the modified Young modulus E_1 = 252.7 GPa (which is used in the thin-walled beam theory because of the assumption of the beam wall contour constant length) the results from Table 1 were combined with the Poisson ratio assumed based on the [4] as 0.3.

The critical load was computed as the smallest root of the polynomial shown in equation (3), see also [2, 5]. The formula on the left hand side of the equation is the determinant of the stiffness matrix created by the 2nd order theory with the assumption of axial compression of the bar and the symetry of the cross-section:

$$P^3\left(r^2-\eta_{2A}{}^2\right)-P^2\left(\left(P_\omega+P_2+P_3\right)r^2-P_3\eta_{2A}{}^2\right)+ \\ +Pr^2\left(P_2P_3+P_2P_\omega+P_3P_\omega\right)-P_2P_3P_\omega r^2=0 \quad (3)$$

Where the symbols were adopted as in [2].The following types of boundary conditions were analysed (Table 3):

1. bar fixed at each end ($\mu_1 = \mu_2 = \mu_3 = 0.5$),
2. elastic boundary conditions at each end according to [2, 6] ($\mu_1 = \mu_2 = \mu_3 = 0.65$),
3. mixed boundary conditions: fixed rotation about the axis η_1 (longitudinal), allowed rotation about the η_3 axis, mixed boundary conditions for the η_2 axis: $\mu_1 = 0.5$, $\mu_2 = 1.0$, $\mu_3 \in [0.5,1.0]$,
4. hinged boundary condition at each end ($\mu_1 = \mu_2 = \mu_3 = 1$).

Table 3. Boundary conditions.

Case 1. fixed			**Case 2. elastic**			**Case 3. mixed**			**Case 4. hinged**		
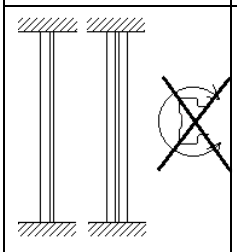											
μ_2	μ_3	μ_1	μ_2	μ_3	μ_1	μ_2	μ_3	μ_1	μ_2	μ_3	μ_1
0.5	0.5	0.5	0.65	0.65	0.65	1.0	0.7	0.5	1.0	1.0	1.0

It was noted that with mixed boundary conditions the value of μ_3 when taken from interval [0.5, 1] has no influence on the results. In the elastic-plastic buckling range the load capacity of analyzed bar was approximated with the Johnson-Ostenfeld parabola:

$$P_{kr} = A\left(R_e - \frac{R_e - R_H}{l_{gr}{}^2} l^2\right), \quad (4)$$

Where the limit length (l_{gr}) value can be found by intersecting the linear buckling curve with the value of $P_H = R_H A$. The obtained limit lengths are shown in Table 4, the values of critical load with respect to bar's length are shown in Figure 3.

Table 4. Limit lengths [cm].

Thinned, not-rounded corners				**Thinned, rounded corners**			
fixed	hinged	mixed	elastic	fixed	hinged	mixed	elastic
355.1	177.5	205.3	273.1	338.3	169.1	200.4	260.2
Full, not-rounded corners				Full, rounded corners			
fixed	hinged	mixed	elastic	fixed	hinged	mixed	elastic
345.5	172.8	196.9	265.8	329.3	164.6	192.2	253.3

By comparing the minimal results (obtained for the bar with thinned cross-section and rounded corners) with the maximal results (obtained for the filled bar with not-rounded

corners) it can be observed that the difference between both results reach up to 15% of maximal value. Analysing the results with respect to boundary conditions shows that the difference between mixed and hinged boundary conditions disappears with increasing length of the bars – which can be justified by reducing the influence of torsion in the cases of flexural-torsional buckling (the buckling mode of the bar with mixed boundary conditions is determined as flexural, while for the hinged support as flexural-torsional).

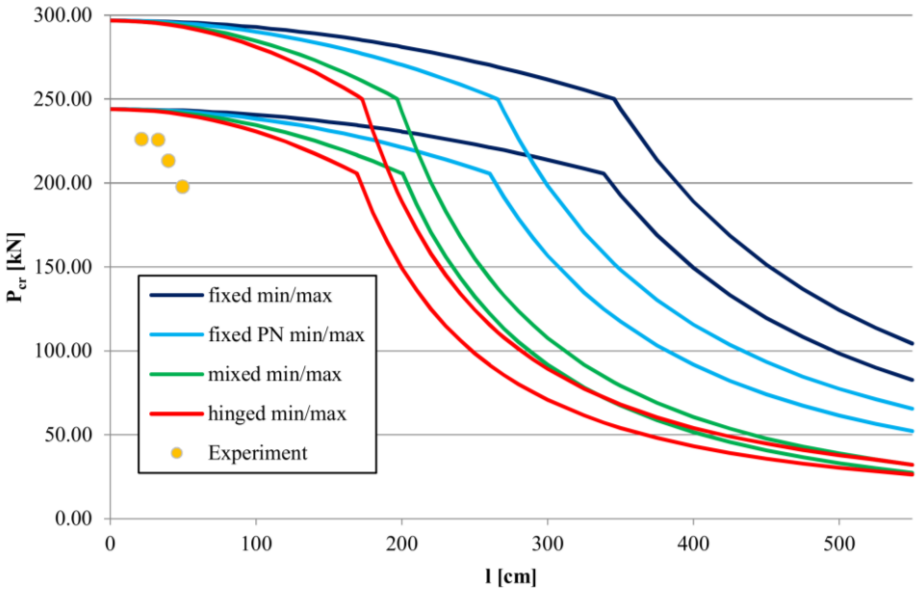

Fig. 3. Limit load for elastic-plastic buckling with respect to element's length.

4 FEM analysis description

As a verification of theoretical approach multiple FEM models, representing bars of multiple lengths, were created, and a parametric study was carried out in order to create the function of compressive bearing capacity of a bar with respect to its length. Only the hinged boundary conditions (compare Table 3 – Case 4) were taken into account.

4.1 FEM model

Each FEM model consisted of multiple repeated modules of 5 cm length joined together by merging the coincident nodes. Total length of the bars used for parametric study varied from 5 to 500 cm - 32 models were analysed.

Each module consisted of 5080 linear shell elements S4R and 82 linear shell elements S3 [7, 8]. The number of variables in the models (DOFs) varied from 32k to 3160k. The material used for constitutive relationship was a linear-elastic material with Huber-Mises plasticity combined with isotropic hardening [9], the parameters of which were adjusted based on the laboratory uniaxial tensile test.

At each end of the bar the boundary conditions were prescribed by applying the displacement load to the point obtained by projecting the bar's center of mass onto the extreme cross-section (see points C-1 and C-2 in Figure 4). All of the nodes belonging to

the extreme cross-section were then connected with corresponding point via MPC beam constraint, thus creating a rigid body. For the FEM analysis only the hinged boudary conditions where applied – each end of the bar had the translations in x, y and z direction, as well as the rotation alongside z axis, restricted (with the displacement load in the z direction). The FE mesh of a module with the location of aforementioned points is shown in Figure 4.

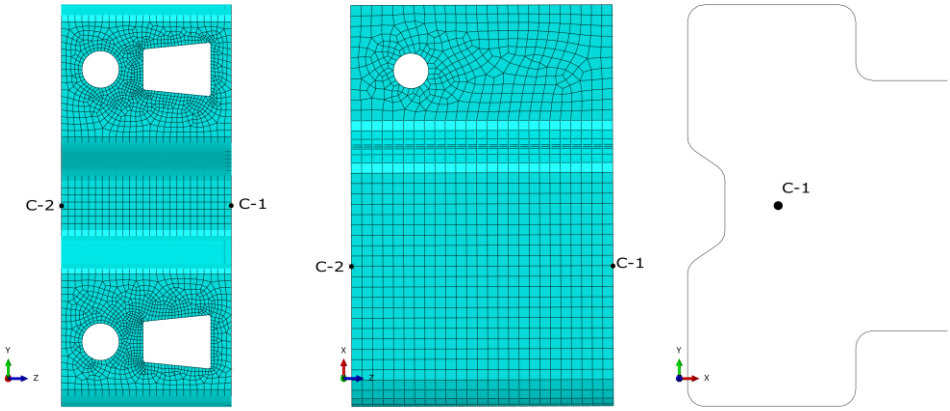

Fig. 4. FEM mesh of the single module with the position of center of mass.

4.2 Analysis

Two sets of analysis were performed: a set of eigenvalue buckling analysis (LBA), where plasticity was not taken into account and only the first critical loads were measured; and a set of quasi-static analysis with elasto-plastic constitutive relationships (GMNA) and the displacement load described in section 4.1. In the latter analysis the maximum force carried by the bar was calculated as the compressive bearing capacity. In each analysis the large displacement theory was used (NLGEOM option, see [8, 9]).

5 Comparison of numerical and analytical results

All the results presented in this section are for the bars with boundary conditions described as Case 4. Graph in Figure 5 shows the comparison of the buckling curves (limit load with respect to the length of the bar) obtained from the eigenvalue buckling FEM analysis with the one calculated analytically as shown in section 3. Bigger diversity can be seen for bars of smaller slenderness – as the use of shell elements in FEM analysis allows to consider local buckling in the walls of the structure.

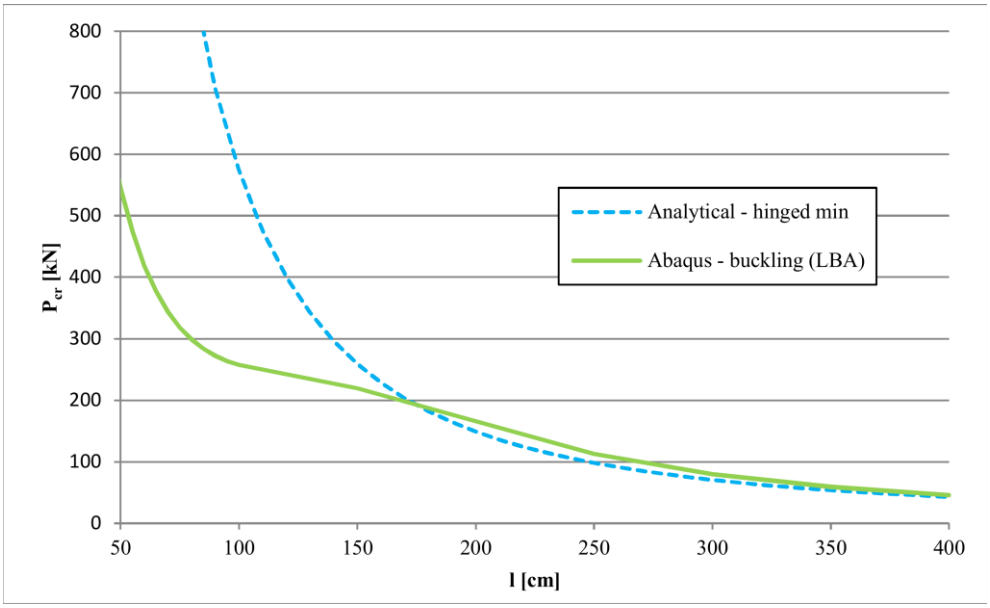

Fig. 5. Results from FEM (LBA) analysis compared to the theoretical results.

Figure 6 shows the load capacity of the bars with respect to their lengths based on the results of quasi-static FEM analysis and compares it to the analytical and experimental results. Here both the elastic and plastic material properties were taken into account. The analytical and numerical results show fine convergence, especially for bars of larger slenderness. Comparison with the results of eigenvalue buckling analysis shows the length for which the load capacity can be determined by linear buckling – here around 3.5m.

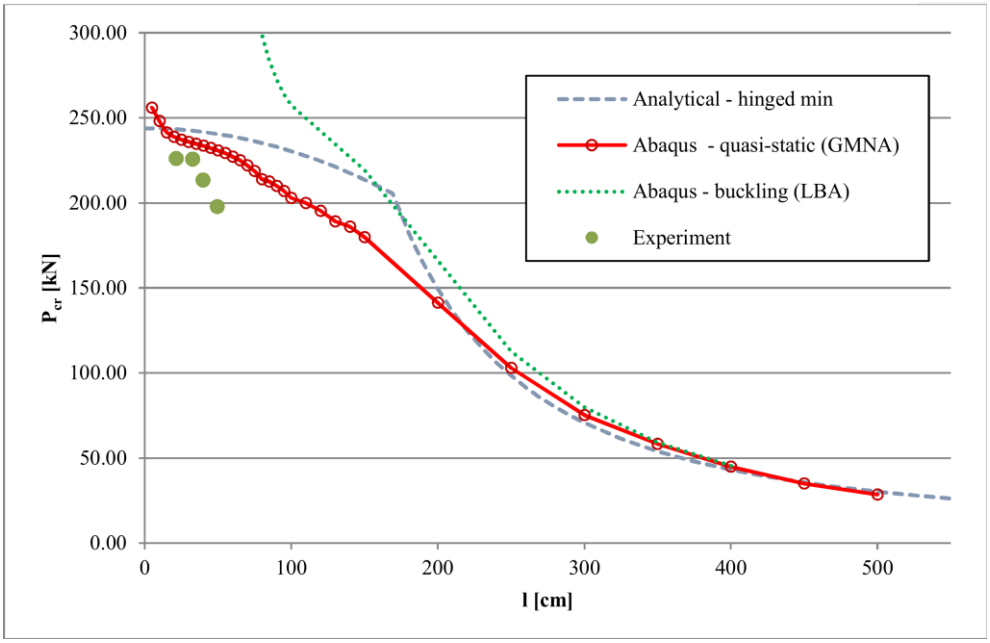

Fig. 6. Results from FEM analysis compared to the theoretical results in case of elastic – plastic buckling.

6 Final remarks and conclusion

The results obtained from FEM solutions showed good convergence with the analytical results by thin-walled beam theory proving that the applied concept of taking into account perforations through thinning of the element wall is rational and leads to proper results. The main divergence between both results appeared for the bars of smaller lengths, as for such lengths the local buckling of the structure walls was more important than global one, and the shell theory would be more appropriate for analytical approach – this conclusion can be taken from both elastic and elastic-plastic analysis. All analysis were made for elements without any imperfections (geometrical shape or boundary conditions imperfections) so the experimental results obtained for tested imperfect models for quite low slenderness ratios should be located below the obtained analytical and numerical results what is visible in graph presented in Figure 6, cf. also [10, 11]. By comparing the buckling load (in the range where the global buckling mode is dominant) obtained from the thin-walled beam theory with the buckling load obtained for shell elements in FEM analysis it is clear that thin-walled beam theory gives smaller values of the critical load. What's more these results are closer to the results obtained from quasi-static FEM analysis done for elasto-plastic material.

References

1. PN-EN ISO 6892-1,Polish Standarization Committee, (2010)
2. J.B. Obrębski, Warsaw University of Technology Publishing House, (1991)
3. PN-EN 1993-1-3: 2008 Eurocode 3, (2008)
4. PN-90/B-03200, Polish Committee for Standarization Measures and Quality, (2008)
5. J. Mutermilch, A. Kociołek, Warsaw University of Technology Publishing House, Warsaw, (1964)
6. PN-80/B-03200, Polish Committee for Standarization Measures and Quality, (2010)
7. ABAQUS/Standard User's manual, Hibbitt, Karlsson & Sorensen, Inc., Pawtucket, (2000)
8. ABAQUS Theory manual, Hibbitt, Karlsson & Sorensen, Inc., Pawtucket, (2000)
9. S. Jemioło, M. Gajewski, Warsaw University of Technology Publishing House, (2014)
10. M.A Giżejowski, R. Szczerba, M. Gajewski, Z. Stachura, Open Access Journal Elsevier **111**, 254-261 (2015)
11. R. Szczerba, M. Gajewski, M.A. Giżejowski, Journal of Civil Engineering, Environment and Architecture **JCEEA-62-03-t2**, 425-438 (2015)